Normal and diseased personal eye modeling using age-appropriate lens parameters

Ying-Ling Chen, [1,*] L. Shi,[1] and J. W. L. Lewis,[1] and M. Wang[2]

[1]Center for Laser Applications, University of Tennessee Space Institute, 411 B. H. Goethert Parkway, Tullahoma, Tennessee, 37388, USA
[2] Wang Vision Institute, Nashville, Tennessee, 37203, USA
[*] ychen@utsi.edu

Abstract: Personalized eye modeling of normal and diseased eye conditions is attractive due to the recent availability of detailed ocular measurements in clinic environments and the promise of its medical and industrial applications. In the customized modeling, the optical properties of the crystalline lens including the gradient refractive index, the lens bio-geometry and orientation are typically assigned with average lens parameters from literature since typically they are not clinically available. Although, through the optical optimization by assigning lens parameters as variables, the clinical measured wavefront aberration can be achieved, the optimized lens biometry and orientation often end up at edges of the statistical distribution. Without an effective validation of these models today, the fidelity of the final lens (and therefore the model) remains questionable. To develop a more reliable customized model without detailed lens information, we incorporate age-appropriate lens parameters as the initial condition of optical optimization. A biconic lens optimization was first performed to provide a correct lens profile for accurate lower order aberration and then followed by the wavefront optimization. Clinical subjects were selected from all ages with both normal and diseased corneal and refractive conditions. 19 ammetropic eyes (+ 4D to −11D), and 16 keratoconus eyes (mild to moderate with cylinder 0.25 to 6D) were modeled. Age- and gender-corrected refractive index was evaluated. Final models attained the lens shapes comparable to the statistical distribution in their age.

© 2012 Optical Society of American

OCIS codes: (330.4060) Vision modeling; (330.0330) Vision, color, and visual optics; (330.4460) Ophthalmic optics and devices; (170.4580) Optical diagnostics for medicine; (170.4460) Ophthalmic optics and devices.

References and links

1. A. Gullstrand, "The optical system of the eye," in *Physiological Optics* 3rd ed., H. von Helmholtz (Hamburg, Voss, 1909), **1**, 350–358.
2. W. Lotmar, "Theoretical eye model with aspherics," J. Opt. Soc. Am. **61**(11), 1522–1529 (1971).
3. R. Navarro, J. Santamaría, and J. Bescós, "Accommodation-dependent model of the human eye with aspherics," J. Opt. Soc. Am. A **2**(8), 1273–1281 (1985).
4. H. L. Liou and N. A. Brennan, "Anatomically accurate, finite model eye for optical modeling," J. Opt. Soc. Am. A **14**(8), 1684–1695 (1997).
5. R. Navarro, L. González, and J. L. Hernández-Matamoros, "On the prediction of optical aberrations by personalized eye models," Optom. Vis. Sci. **83**(6), 371–381 (2006).
6. P. Rosales and S. Marcos, "Customized computer models of eyes with intraocular lenses," Opt. Express **15**(5), 2204–2218 (2007).
7. Y.-L. Chen, B. Tan, K. Baker, J. W. L. Lewis, T. Swartz, Y. Jiang, and M. Wang, "Simulation of keratoconus observation in photorefraction," Opt. Express **14**(23), 11477–11485 (2006).
8. C. Winkler von Mohrenfels, A. Huber, B. Gabler, W. Herrmann, A. Kempe, C. Donitzky, and C. P. Lohmann, "Wavefront-guided laser epithelial keratomileusis with the wavelight concept system 500," J. Refract. Surg. **20**(5), S565–S569 (2004).

9. J. Castanera, A. Serra, and C. Rios, "Wavefront-guided ablation with Bausch and Lomb Zyoptix for retreatments after laser in situ keratomileusis for myopia," J. Refract. Surg. **20**(5), 439–443 (2004).
10. D. Y. Lin and E. E. Manche, "Custom-contoured ablation pattern method for the treatment of decentered laser ablations," J. Cataract Refract. Surg. **30**(8), 1675–1684 (2004).
11. J. B. Almeida and A. M. Garcia, "Theoretical calculation of a contact lens thickness designed to correct the eye's monochromatic aberrations," Optom. Vis. Sci. **82**(1), 59–63 (2005).
12. J. Marsack, T. Milner, G. Rylander, N. Leach, and A. Roorda, "Applying wavefront sensors and corneal topography to keratoconus," Biomed. Sci. Instrum. **38**, 471–476 (2002).
13. W. N. Charman, "Wavefront technology: past, present and future," Cont. Lens Anterior Eye **28**(2), 75–92 (2005).
14. D. A. Atchison, E. L. Markwell, S. Kasthurirangan, J. M. Pope, G. Smith, and P. G. Swann, "Age-related changes in optical and biometric characteristics of emmetropic eyes," J. Vis. **8**(4), 29 (2008).
15. M. Dubbelman and G. L. Van der Heijde, "The shape of the aging human lens: curvature, equivalent refractive index and the lens paradox," Vision Res. **41**(14), 1867–1877 (2001).
16. D. A. Goss, H. G. Van Veen, B. B. Rainey, and B. Feng, "Ocular components measured by keratometry, phakometry, and ultrasonography in emmetropic and myopic optometry students," Optom. Vis. Sci. **74**(7), 489–495 (1997).
17. D. A. Atchison, "Optical models for human myopic eyes," Vision Res. **46**(14), 2236–2250 (2006).
18. S. Stenstrom, "Investigation of the variation and the correlation of the optical elements of human eye Part V—Chapter III (D. Woolf, Trans.)," Am. J. Optom. Arch. Am. Acad. Optom. **25**, 438–449 (1948).
19. N. A. McBrien and D. W. Adams, "A longitudinal investigation of adult-onset and adult-progression of myopia in an occupational group. Refractive and biometric findings," Invest. Ophthalmol. Vis. Sci. **38**(2), 321–333 (1997).
20. R. Scott and T. Grosvenor, "Structural model for emmetropic and myopic eyes," Ophthalmic Physiol. Opt. **13**(1), 41–47 (1993).
21. H. M. Cheng, O. S. Singh, K. K. Kwong, J. Xiong, B. T. Woods, and T. J. Brady, "Shape of the myopic eye as seen with high-resolution magnetic resonance imaging," Optom. Vis. Sci. **69**(9), 698–701 (1992).
22. L. A. Jones, G. L. Mitchell, D. O. Mutti, J. R. Hayes, M. L. Moeschberger, and K. Zadnik, "Comparison of ocular component growth curves among refractive error groups in children," Invest. Ophthalmol. Vis. Sci. **46**(7), 2317–2327 (2005).
23. A. Cook, S. White, M. Batterbury, and D. Clark, "Ocular growth and refractive error development in premature infants without retinopathy of prematurity," Invest. Ophthalmol. Vis. Sci. **44**(3), 953–960 (2003).
24. D. O. Mutti, G. L. Mitchell, L. A. Jones, N. E. Friedman, S. L. Frane, W. K. Lin, M. L. Moeschberger, and K. Zadnik, "Axial growth and changes in lenticular and corneal power during emmetropization in infants," Invest. Ophthalmol. Vis. Sci. **46**(9), 3074–3080 (2005).
25. F. C. Pennie, I. C. Wood, C. Olsen, S. White, and W. N. Charman, "A longitudinal study of the biometric and refractive changes in full-term infants during the first year of life," Vision Res. **41**(21), 2799–2810 (2001).
26. S. Ziylan, D. Serin, and S. Karslioglu, "Myopia in preterm children at 12 to 24 months of age," J. Pediatr. Ophthalmol. Strabismus **43**(3), 152–156 (2006).
27. Y.-L. Chen, B. Tan, L. Shi, J. Lewis, M. Wang, and K. Baker, "The shape of aging lens," Invest. Ophthalmol. Vis. Sci. **51**, E-Abstract 4593 (2010).
28. L. Tong, S. M. Saw, D. Tan, K. S. Chia, W. Y. Chan, W. H. Chua, and C. Y. Hong, "Sensitivity and specificity of visual acuity screening for refractive errors in school children," Optom. Vis. Sci. **79**(10), 650–657 (2002).
29. J. F. Koretz, P. L. Kaufman, M. W. Neider, and P. A. Goeckner, "Accommodation and presbyopia in the human eye--aging of the anterior segment," Vision Res. **29**(12), 1685–1692 (1989).
30. A. V. Goncharov and C. Dainty, "Wide-field schematic eye models with gradient-index lens," J. Opt. Soc. Am. A **24**(8), 2157–2174 (2007).
31. A. V. Goncharov, M. Nowakowski, M. T. Sheehan, and C. Dainty, "Reconstruction of the optical system of the human eye with reverse ray-tracing," Opt. Express **16**(3), 1692–1703 (2008).
32. C. E. Campbell, "Nested shell optical model of the lens of the human eye," J. Opt. Soc. Am. A **27**(11), 2432–2441 (2010).
33. G. Smith, "The optical properties of the crystalline lens and their significance," Clin. Exp. Optom. **86**(1), 3–18 (2003).
34. J. Rozema, D. Atchison, and M. Tassignon, "Statistical eye model for normal eyes," Invest. Ophthalmol. Vis. Sci. **52**, 4525–4533 (2011).

1. Introduction

Analytical eye models have been developed for over a century [1–5]. Traditional models use the average measured optical parameters and characteristics of healthy emmetropic adults. These models are valuable for the study of visual optics and for applications for common vision correction. However, these models are rotationally symmetric and cannot represent any individuals in the general population. Advances of ophthalmic technology in the last decade

have made available detailed clinically measured ocular data for customized eye modeling [5–7]. Customized modeling for normal and diseased eyes offers current and potential assistance for ocular surgery [8–10] and for the design of customer-tailored spectacle-, contact-, or intraocular lens [11–13]. With additional modifications, these models can predict visual changes under varied environmental and physical conditions. Furthermore, ophthalmic measurement simulations using customized models of diseased eyes suggest a potentially versatile method for medical training as well as for the development of new instruments.

Today the most common and attainable clinical measurement data that are used for constructing customized schematic models are the 3-dimensional anterior segment structure data acquired from Pentacam or Orbscan instruments, the ocular wavefront aberration (WF) from any typical wavefront aberrometer, and the ocular element distances obtained from A-scan or IOL-Master. With these clinical data, a customized optical eye model can be constructed using contemporary optical software such as ZEMAX or Code V [5]. Optical optimization was performed to alter the unknown lens parameters to achieve the eye's wavefront aberration. Questions regarding these models' fidelity arise from the shortage of information of the crystalline lens of the individual eyes. Frankly, the variable lens parameters outnumber largely the required iteration variables for wavefront optimization.

In order to refine the initial lens condition for each individual, the literature of lens parameters and considered factors of age, gender, and refractive error was first reviewed and summarized. To test the lens-refining scheme we include 35 eyes over an age range of 40 + years that have normal lens but possess a large variation of normal and diseased corneal and ametropic conditions. We then constructed an initial model with clinical biometry data and age- and gender-corrected lens biometry. Optical computational optimizations on assigned lens parameters were performed in two stages to approach the individual's wavefont aberration. The equivalent refractive index was age- and gender-corrected using results from the Atchison and Dubbelman studies [14, 15], and the optimization results were compared to statistics. This study is essential to advance toward more reliable and realistic personalized eye modeling for future development and applications.

2. Personalized eye modeling

Subject

This study used 35 eyes examined in the Wang Vision Institute in Nashville. Nineteen of the 35 eyes are normal healthy eyes. They include two emmetropic, seven myopic, three hyperopic, and seven myopic astigmatic eyes. Spherical equivalent values range from −11.25 D to + 4.25 D, and the range of astigmatism are from 0 to 3D. Fifteen of these 19 eyes have best corrected visual acuity (BCVA) of 20/20, one is 20/25, and three are 20/30. The remainder (sixteen) of eyes exhibit mild to moderate keratoconus (KC and FFKC) with spherical equivalent values that range from −7.9 D to −0.1 D. Astigmatism ranges from 0.5 to 6 D. For the KC and FFKC eyes, there is no known abnormality other than that of the cornea. Four of these 16 eyes have BCVA of 20/20, two are 20/25, seven are 20/30, and three are 20/40. Four of these KC eyes have cylindrical refractive error less than 1 D. The patients' ages range from 24 to 68 year old (41.5 +/− 12.6 years old).

Ophthalmic patient data

Anterior and posterior corneal topographies from Pentacam were utilized in the modeling. The spatial increments of these elevation maps were 0.1 mm in X- and Y- transverse dimensions, and 0.001 mm in Z-dimension. Cornea thickness (CT), anterior chamber depth (ACD), and the displacement (dx, dy) of the apex-to-center of the pupil were also acquired from Pentacam. Three measurements of wavefront aberration (WF) data were acquired from Wavescan. The modeling selected the WF data set with largest pupil size. If pupil sizes were the same in WF data, the one with smallest high-order aberration was chosen. IOL-Master

and/or A-Scan were used to measure ocular axial length (AL). Lens thickness (LT) was obtained using A-Scan.

Crystalline lens parameters

To include in the lens model the dependence of the lens parameters on age, gender, and refractive error, we reviewed 36 lens biometry studies. The results of this review are shown in Figs. 1-3.

To our knowledge, no evidence has been found of correlation between sphero-cylindrical refractive error and any of lens properties in adults, children, and infant populations [16–26]. Thus, the patient's refractive error condition would not influence lens parameters in the modeling. The age, however, is one significant factor for lens characteristics [27]. These age-dependent equations were plotted in dashed lines in Figs. 1, 2, and 3. In Fig. 1, the plot on the left compares 18 studies of lens thickness. The age-trend was significant and showed rapid decrease of thickness from ~4mm at infancy to the minimum value ~3.4mm at 10 years old. After the age of 10, there was a slower rate of increase on lens thickness with age. The solid black line marks the fitted polynomial result [27]. Correlation of gender to lens thickness was investigated by Atchison in 2008 [14]. No significant correlation was found. Thus, we use the same age-dependent equation for both genders. Systematic inconsistency between measuring instruments was investigated by Atchison [14], Tong [28], and Koretz in [29] in 2008, 2002, and 1989, respectively, and a difference of lens thickness of up to 0.2 mm was estimated. This deviation range of +/− 0.2mm is illustrated by the grey band in the plot.
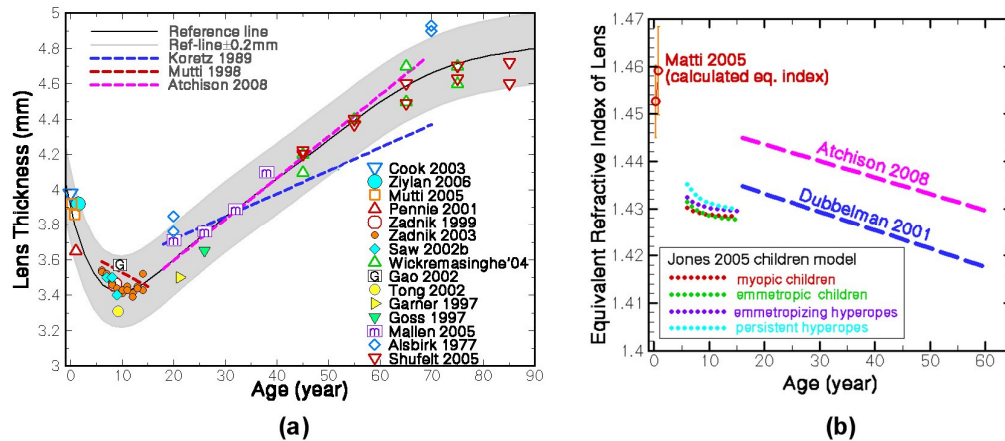

Fig. 1. (a) Comparison of studies of age-correlation of lens thickness. The fitted curve (black) is: $y(x) = 3.9 - 0.127x + 0.0116x^2 - (4.49E-4)x^3 + (9.62E-6)x^4 - (1.15E-7)x^5 + (7.14E-10)x^6 - (1.8E-12)x^7$; (b) Comparison of studies on age-dependence of equivalent refractive index.

For the lens index of refraction, although Liou and Brennan [4] in 1997 and Goncharov and Cambell in 2007, 2008 and 2010 [30–32] modeled the more realistic gradient index (GRIN) to mimic the human lens, an 'equivalent' constant index has often been used for simplification to describe the actual gradient index. The GRIN index typically is around 1.40-1.42 at the core and ~1.35 at outer shell. In comparison, the equivalent refractive index is higher in magnitude in order to support sufficient refraction on the lens surfaces of same curvatures. The Navarro 1985 model [3] uses a lens index of 1.42 for the relaxed eye. In 2008 Atchison [14] used Purkinje imaging applied to the 4-surface eye model to describe the equivalent refractive index as a function of age and found a significant trend: $n = 1.4506-0.00035*(Age)$ (adjusted $r^2 = 0.21$, n = 102, p<0.001). In comparison, Dubbelman in the earlier 2001 study [15] obtained $n = 1.441-0.00038*(Age)$. In 2005 Jones found age-dependent crystalline lens index for US children 6 to 15-years old [22], and Matti 2005

provides data of infants at 3 and 9 month old that were derived to match the measured refractive error [24]. The age-trend is significant, p<0.0001. Error bars are included. On the right of Fig. 1, these results are shown for comparison.

Many studies of lens radii of curvature are illustrated in Fig. 2, and the age-trend shows an extremum around the teenage period. Similarly, reference lines by polynomial fitting [27] and the estimated derivation ranges (grey bands) were plotted for comparison. In the Atchison 2008 study, no significant radii differences between genders were found. Therefore, we adopted gender-independent reference lines.
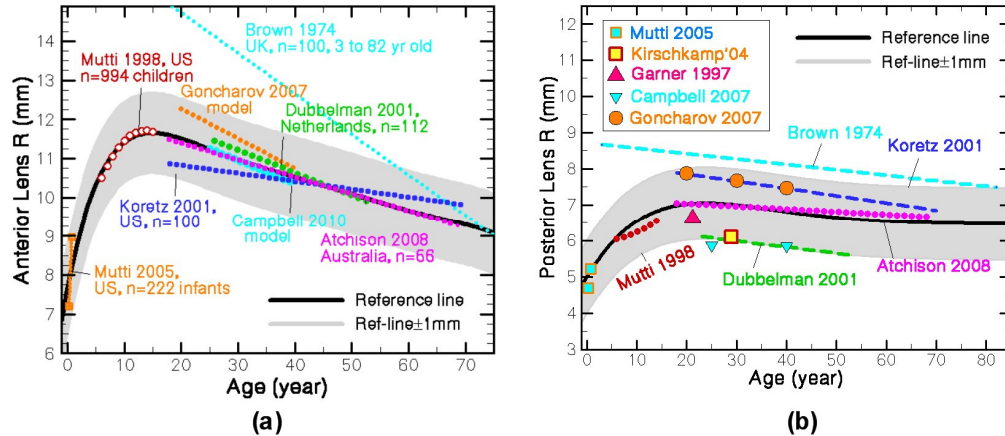
Fig. 2. Comparisons of studies of age-correlations of anterior (a) and posterior (b) lens radii of curvature. The radii of curvature on lens surfaces were free variables during the optical optimization of the customized models. Anterior fitted line (black): $y = 7.66 + 0.76x-(5.32E-2)$ $x^2 + (1.75E-3)x^3-(3.08E-5)x^4 + (2.77E-7)x^5 + (9.96E-10)x^6$; Posterior fitted line: $y = 5.09 + 0.234x-(9.37E-3) x^2 + (1.63E-4)x^3-(1.32E-6)x^4 + (4.12E-9)x^5$.

Conic constants of both the anterior and posterior lens surfaces have been reported in a few studies [15, 17, 33]. As shown in Fig. 3, the reported values of the conic constant range between 0 and −6 for anterior lens surface and between + 2 to −5 for posterior surface. Although plotted as functions of age in these studies, no significant correlation to age was found. In the personalized models of this current work, conic constants were therefore assigned to be free iteration variables during the biconic lens surface optimization.
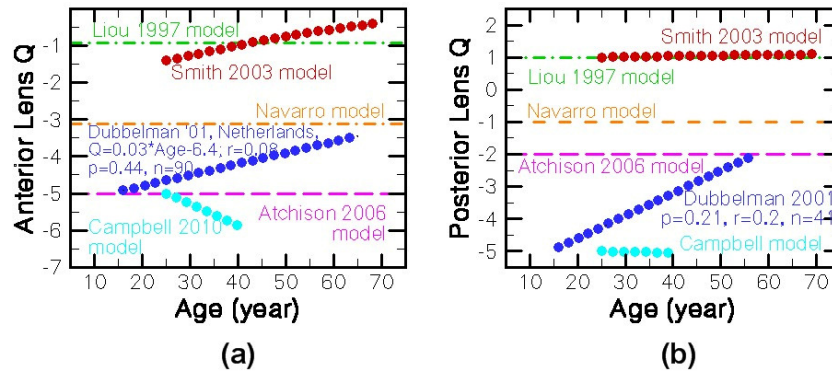

Fig. 3. Comparisons of studies of age-correlations asphericity of anterior (a) and posterior (b) lens surface. No significance of age-correlation was found in any of these studies. The conic constants on lens surfaces were free variables during the optical optimization of the customized models.

Customized eye modeling

For eye modeling using average ocular parameters, a very comprehensible, step-by-step article by Tocci, "How to model the human eye in Zemax", can be found in the Zemax Knowledge Base website. Personalized eye modeling using clinical data was described in depth by Navarro in 2006 [5]. This section our study describes the differences with previous methods and provides additional details of the lens modeling.

ZemaxTM optics code, (ZEMAX Development Corporation, Bellevue, WA, USA), was used in this modeling. For personalized modeling, two essential and distinct optical optimizations steps must be executed. The first is a biconic surface optimization that intended to approach the accurate lens profile and the eye's low-order aberration. The second is to include microscopic perturbation on lens property to achieve the total ocular wavefront aberration. Without a carefully tailored lens profile optimization in the first step, the Zernike optimization that followed would most likely obtain the customer's measured wavefront aberration regardless of the significance of the deviation of the lens profile from the real one, thereby giving a false sense of success.

The data input description follows: Using Zemax, eye elements/surfaces were constructed 'backward' from retina to cornea similar to how the wavefront aberration was measured on the return path. In this orientation, the cardinal coordinates in Zemax were aligned to clinical presentation of topography and wavefront. We assumed the keratometric axis of topography to be parallel to the visual axis and that the Z-axis in Zemax was closely aligned to the chef ray through the pupil center. The biconic-Zernike surface type in Zemax was assigned to both crystalline lens surfaces. Radii of curvature and conic constants from the Navarro model [3] were given as initial values. The lens was rotated 5 degrees (Y-axis), toward temporal side, from the center of lens to compensate for the visual axis. No translation was applied to the lens element. Grid-Sag surface type was assigned for both corneal surfaces. Refractive indices of cornea and aqueous humor were known to have no age-correlation. Wavelength-dependent (dispersive) refractive indexes of cornea, aqueous humor, vitreous humor, and lens were adopted from the Navarro model [3], and the Conrady formula was used in Zemax. The lens index was then adjusted with age-correction using Atchison's equation [14] and Dubbelman's result [15] that were described earlier. Measured ocular biometry data (ACD, AL, LT, CT, dx, dy) were entered into the model.

Because of the demand of an absolutely minimal RMS wavefront error of the final eye model, the initial Pentacam topography data was extended from 1 to 0.01 micron meter precision. To retain the fidelity to the topographic profiles, we decompose the elevation raw data up to 25th order of Zernike terms and reconstruct the elevation maps from these coefficients. When rounded up 2 digits, the new topographies are equivalent to the original clinical data in every data point throughout the topographies. The two customized corneal surfaces were then imported without rotation to the Grid-Sag surfaces in the model. A spatial translation, (-dx, -dy), relative to the pupil center was assigned.

A Zernike phase plate was inserted in the ray-tracing sequence after the anterior cornea at the exit pupil plane (entrance pupil of the eye). The wavefront aberration map of the patient was imported to this surface, and the optical stop was assigned to it with the maximum size of the measured WF map. After the phase plate, an ideal thin lens with focal length of 100 m was inserted in front of the eye. The final image plane was placed at 100 m so that the optimization would ensure an eye model with the clinical measured wavefront aberration.

We investigated the related orientation between the 2 sets of clinical data, topographies and wavefront, by assigning free variables on 2 tilting angles (x- and y-axes) of the anterior elements and one rotation variable (z-axis) on the wavefront phase plate. A merit function was provided to minimize the residual RMS wavefront error with 64X64 papillary iteration rays. Constraints of +/− 5 degrees and +/− 10 degrees were assigned. We found the orientation adjustment to be insignificant. The initial conditions affected the results by

indicating multiple and small local minima. The sensitivity is low to not only the normal ammetropic eyes but also the keratoconus eye models. Therefore, other than the translational alignment according to the pupil centers indicated on the 2 measurements, the orientations of the corneal topographies and the wavefront phase plate were modeled to be untilted from the X-Y plane or rotated along the Z-axis.

During the first step of optimization, one objective was to approach parameter values that were consistent with the statistically correct lens profile for the age and gender of the this specific individual's age and gender; this optimization should produce parameters that were altered to yield the major ocular 4th- and 2nd- order aberrations. Biconic (elliptical) surfaces were assigned for the lens, and a coordinate rotation (tilt) on Z-axis was applied to the whole lens element related to the center location. This allowed the lens to have cylinder power in an arbitrary meridian after optimization. Although a simpler bi-quadric surface could accomplish the purpose, the bi-conic surface type is supported by Zemax without additional complication.

Since the gradient index of the natural human lens structure contributes to a degree of refraction and spherical aberration (SA), in the use of a constant refractive index lens, an equivalent index that is higher than the mean index and additional asphericity on the lens surfaces are expected to accommodate the loss of refraction and SA. We assigned five variables for optimization: the meridian angle, the two radii of curvature on the steepest and flattest meridians of the posterior lens surface, and the two conic constants on the two meridians of the same surface. The two radii and two conic constants on the anterior lens surface were assigned to "pick up" the values of the posterior surface with assigned constant ratios. The specific ratios for conic constants to pickup were 1. The ratio between anterior and posterior radii was age-dependent. It was assigned with the ratio of the two age-dependent reference lines in the two radii plots in Fig. 2.

We used real ray aiming, a selected wavelength at 0.785 um of the Wavescan and used default merit function with setting of RMS/spot radius/Centroid/Rectangular array 20X20. After the biconic 5-variable optimization, a Zernike sag optimization to 13th-order was performed on the posterior lens surface. After this optimization, the wavefront aberration of the eye model converged to the clinical measured data with an RMS error about 0.01 wave. Shown in Fig. 4 is the RMS wavefront error along the optimization steps. The biconic len profile optimization step significantly reduced the residual between total wavefront and corneal wavefront. The magnitude of final RMS error depends dominantly on the pupil size.
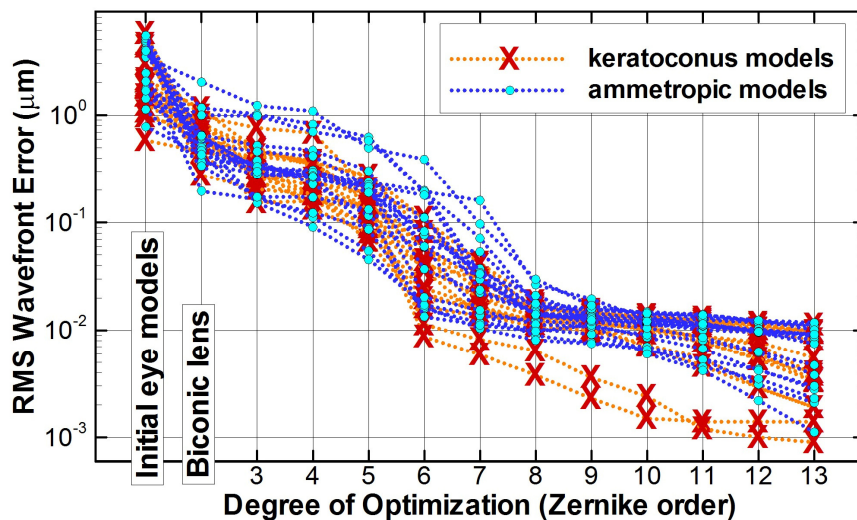

Fig. 4. RMS wavefront error of the eye models along the optical optimization steps.

3. Results and discussion

The results of biconic surface optimization were presented in Figs. 4, 5, and 6. The radii (of curvature) of anterior lens and the posterior surfaces were plotted on the left and the right of each figure respectively. On the background of each plot, a reference black line and the grey band describe the average age trend of deviation from multiple studies that was described earlier. Symbols described the results of the 35 customized models. Blue circles represented the 19 normal eyes, and red triangles were the 16 keratoconus eyes. Both steepest and flattest radii of curvatures of the lens surface were plotted. Linear fittings were given in dashed lines for both normal (blue dash) and the keratoconus (red dash) groups.

In Fig. 5, Dulbbelman's age-dependent equivalent refractive index (see the blue dashed line in right plot of Fig. 1) was used in the modeling. The optimization result of lens radii tended to be smaller than the values that were reported from majority of literature including Dulbbelman's (see reference line and also compare to Fig. 2). The lens surfaces were steeper, and the deviation from the average line was worse when age increased toward 70 years. The conic constants after optimization were found in −3.35+/−2.21, a reasonable range compared to publications.
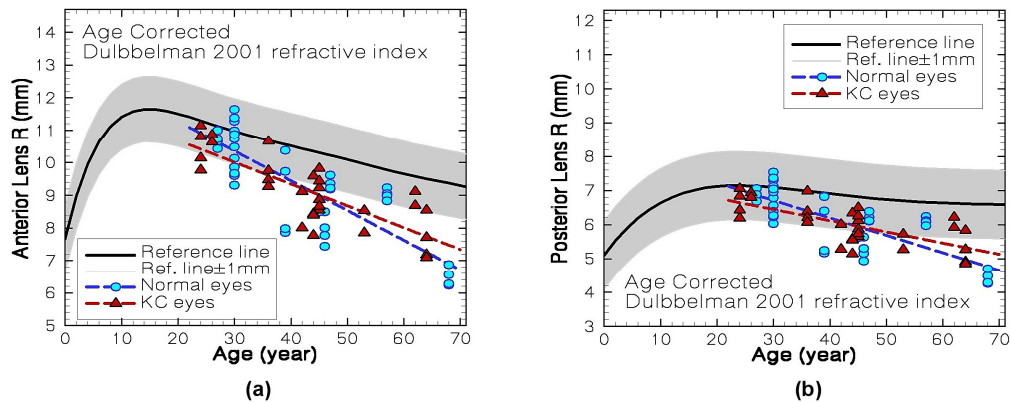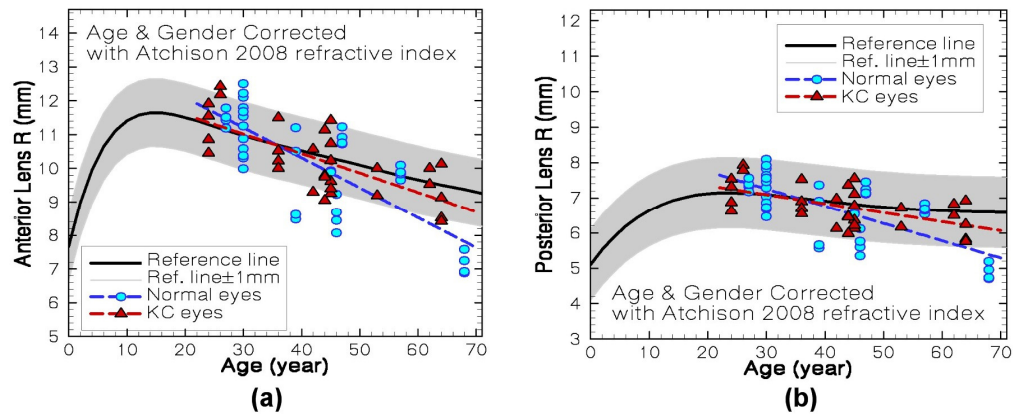

Fig. 5. Optimization results of the radius of curvature of anterior lens surface (left) and posterior surface (right). The lens refractive index of Dulbbelman 2001 [15] study was used in this modeling.

Figure 6 shows results using the refractive index concluded by Atchison's 2008 study for emmetropic eyes. In Atchison's study, not only age-dependency was provided but also gender correlation was given with statistical significance. We included both age- and gender corrections in this set of customized modeling. The refractive index at 555nm was given as 1.4506-0.00035*(Age) and female's (male's) index was then added (subtracted by) 0.0035 from the norm equation. As shown in Fig. 5, the biconic optimization results of lens surfaces' radii in the 35 individuals' eyes showed an exceptionally encouraging agreement compared to the age-related reference line and the statistical distribution that were based on the measured radius values from other publications. Conic constants were found in −3.78 +/− 2.83, which is in agreement with the published range. We noticed that the slopes of the two fitted lines for normal eye group and keratoconus group were slightly steeper than the average line. This difference might suggest a possible over-estimate of the decrease of refractive index with aging, which was −0.00035/year. In a recent Rozema and Atchison publication with 66 eyes [34], the correlation of refractive index with age appeared to be weaker, supporting our finding.

For comparison and further investigation, we performed the three computations: a) use gender- but no age-correction, b) use age- but no gender- correction, and c) use neither age- nor gender-correction but use a constant refractive index that is appropriate for an age of 35

years from Atchison's 2008 equation. We found that the consideration of age and/or gender correlations in refractive index resulted did not provide significantly better fit to the radii statistics. Figure 7 shows results obtained using the constant refractive index for an age of 35 years. Conic constants results were in −4.01 +/− 3.06.

Fig. 6. Optimization results of the radius of curvature of anterior lens surface (left) and posterior surface (right). The lens refractive index of Atchison 2008 study [14] was used in this modeling.
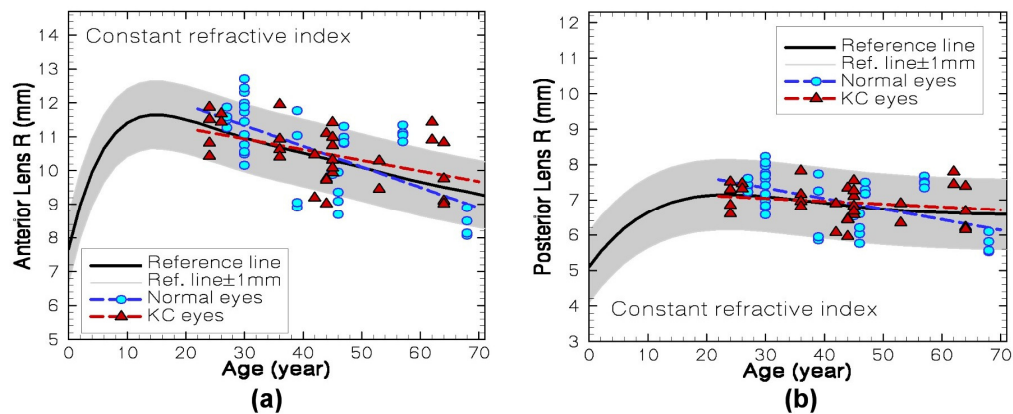

Fig. 7. Optimization results of the radius of curvature of anterior lens surface (left) and posterior surface (right). The 35 years old lens refractive index of Atchison 2008 study [14], n = 43835, was used in this modeling.

4. Summary

To advance the customized eye modeling technology we first summarized and illustrated the aging human lens parameters in comprehensible presentations and incorporated the age-trends in the models. We included 35 eyes from 24 to 68 years old with a wide range of eye conditions to test the implementation of age-related lens features. When adapting equivalent lens refractive index of Atchison's 2008 study, the lens surface radii of curvature and conic constants of the customized models showed good agreement with statistical distribution in their ages. The modeling result from this study also suggests that the equivalent refractive index of the lens has a weaker age and gender correlations in our cohort than that of the reported. Both the keratoconus group and healthy ammetropic eye group generated results comparable to age properties described in reviewed literature, demonstrating the reliability of this modeling method. In the near future, a more realistic gradient index model will be tested and compared with the equivalent index model.

Acknowledgments